

JOURNAL OF ENERGY SYSTEMS

2025, 9(3)



2602-2052 DOI: 10.30521/jes.1723925

Research Article

A novel origami inspired single rotor horizontal axis wind turbine

Ahmad Sedaghat *

Australian University, College of Engineering, Department of Mechanical Engineering, Kuwait, a.sedaghat@au.edu.kw

Bassem Djedi 4

Australian University, School of Aviation, Kuwait, b.djedi@au.edu.kw

Mohamad Hussein Farhat 4

Australian University, College of Engineering, Department of Electrical and Electronics Engineering, Kuwait, m.farhat@au.edu.kw

Mohamad Iyad Al-khiami 😃

 $Australian\ University, College\ of\ Engineering,\ Department\ of\ Civil\ Engineering,\ Kuwait,\ m. alkhiami@au.edu.kw$

Mohamed El Badawy

Australian University, College of Engineering, Department of Mechanical Engineering, Kuwait, m.elbadawy@au.edu.kw

Submitted: 21.06.2025 Accepted: 12.08.2025 Published: 30.09.2025



* Corresponding Author

Abstract: Wh

While several distinct vertical axis wind turbines with low power performance exist for integration in buildings, implementing micro horizontal axis wind turbines in buildings poses challenges due to their visual impacts, noise levels, and risks to flying birds. In this work, seven novel origami rotor designs featuring four internal tubular nozzle shapes and varying inlet/outlet aspect ratios are manufactured using 3D printing and tested in a subsonic wind tunnel under three scenarios: Without a micro-3-phase electric generator, with the generator but no load, and with both generator and a load, across wind speeds ranging from 3.5 m/s to 25 m/s. Results indicate that the designs with an aspect ratio below 3 perform well. Cut-in speeds of 3.5 m/s and 8 m/s are achieved with and without the electric generator, respectively. The rotation speeds range from 25 rpm to 3300 rpm. A maximum voltage of 27.6 V is recorded without load and the maximum power coefficient of 0.0168 is achieved at the tip speed ratio of 0.44 for a micro turbine with a 10 cm diameter. This research further elaborates on the characteristics of the different rotor designs, discusses their respective advantages and shortcomings, and outlines plans for future modification.

Keywords: Bladeless, Environment impact, Horizontal axis, Hubless, Noise reduction, Origami, Single rotor, Wind turbine.

Cite this Sedaghat, A, Djedi, B, Farhat, MH, Al-khiami, MI, El Badawy, M. A novel origami inspired single rotor horizontal axis paper as: wind turbine. *Journal of Energy Systems 2025; 9*(3): 271-291, DOI: 10.30521/jes.1723925

2025 Published by peer-reviewed open access scientific journal, JES at DergiPark (https://dergipark.org.tr/jes)

Nomenclature Descriptions Abbreviations Three Dimensional Outer Diameter Mass flow rate (kg/m3) AC Alternating Current PC Personnel Compute Rotor power (W) RPM P_W R AR Aspect Ratio Revolutions per Minute Wind power (W) BEM Rotor Radius (m) Blade Element Momentum RSM Reynolds Stress Model Turbulent Intensity CAWT Cross Axis Wind Turbine TI Rotor torque (N.m) Computational Fluid Dynamics TSR Tip Speed Ratio Velocity vector (m/s) CFD Variable Speed Wind Turbine CS CV Control Volume VSWT V_{in} Inlet velocity (m/s) $_{V_{out}}^{V_{out}}$ Outlet velocity (m/s) VAWT Vertical Axis Wind Turbine Control Surface DC Direct Current Width Wind speed (m/s) DIY Do-It-Yourself Latin symbols Greek symbols EV Electric Vehicle Inlet area (m²) The correcting factor (-) A_{in} β A_{out} AR Outlet area (m2) Length Tip speed ratio (-) LCD Liquid Crystal Display Aspect Ratio (-) Rotor rotational speed (RPM) ω LCWT Linear Cascade Wind Turbine A_R Rotor area (m2) Air density (kg/m3) LED Light-Emitting Diode dPower coefficient (-) Gulf Cooperation Council GCC Derivation with respect to time dt dA Differential area (m2) Н HAWT Horizontal Axis Wind Turbine Differential volume (m3) $d\mho$ NACA National Advisory Committee for Aeronautics F Force vector (N) Axial force (N) NIMBY Not-In-My-Back-Yard Tangential force (N)

1. INTRODUCTION

1.1. Literature on Small Wind Turbines

The design of large horizontal axis wind turbines (HAWTs) has not significantly changed over years and issues remain challenging, such as lower efficiency at low wind speeds, less power generation in turbulent and fast changing wind, and generation beyond cut-out wind speeds [1]. In contrast, vertical axis wind turbines have operated at such unfavorable wind conditions, yet they possess very low power coefficients. In offshore applications involving a 1 MW vertical axis wind turbine, surge, heave, and pitch are identified as the dominant motions, highlighting the suitability of such platforms for offshore wind energy generation [2].

In urban environments where small wind turbines are utilized, there are uncertainties in power generation due to the complexity of wind profiles because of the morphology of urban buildings [3]. Turbulent intensity (TI) has been shown to be an important factor for its incorporation within a modified Weibull distribution function of wind speeds [3] for better predictability of power generation from small wind turbines.

The blade design of small HAWTs was considered from the perspectives of laboratory test to field operation of market ready products with lesser structural complexity [4]. The new blade designs were investigated under extreme static and dynamic wind loads. The importance of different rotational speeds at a fixed wind speed on power generation was experimentally reported [4]. Integrating cascade wind turbines within a building is challenging and new designs such as linear cascade wind turbine (LCWT) offer solutions particularly at low blade tip speed ratio (TSR) [5]. The design however needs to be installed in an open environment, such as the space between two separate buildings reporting efficiencies of 8% and 12% performances without and with ducted design, respectively [5]. To improve small HAWT performance, several diffuser flanges or lens augmented devices were developed and experimentally assessed. There were attempts to enhance the performance of the diffuser type wind turbines by improving the blade design, claiming theoretically better performance than the Betz limit [6]. A recent study fully explored the literature of such augmented devices and tested a variety of geometries including annular, cylindrical, and conical shapes. The study concluded that none of these devices can improve the HAWT performance beyond the Betz limit [7]. However, the best performance was obtained for smaller flanges with a total C_p value of 0.576.

Full scale wind tunnel testing of small VAWTs is highly important for the true evaluation of these wind turbines in terms of cut-in wind speed, power generation, and the measure of power coefficient. The wind tunnel testing of a Darrius type wind turbine revealed that a standard Darrius wind turbine has a cut-in wind speed of 10 m/s. However, with blade design improvements, this speed was reduced to 6 m/s [8]. But in the improved Darrius design the maximum power coefficient hardly reached 0.16 [8]. However, the recent review of the last decade research on CFD enhancements of Darrius type wind turbines, with leading-edge protuberances, indicates that the power coefficient can be enhanced up to 25% [9]. A novel conical multiple bladed small HAWT design with different pitch angles and conical angles was explored using experimental and computational methods [10]. The new concept started generating power at a cut-in wind speed of 4 m/s and achieved a maximum power coefficient of 0.47 using 30 blades [10]. Although the design is more efficient compared to other small wind turbines, it is not preferred in practical terms due to cost of production. A bio-inspired design based on a fish-tail shape was investigated in a Savonius type VAWT wind turbine computationally and achieved the maximum power coefficient of 0.267 [11]. Computational tools were also developed to investigate the casing of the Savonius wind turbines. The wind turbines indicated a similar maximum power coefficient below 0.27 can be achieved [12]. Based on experimental measurements, it appears that standard Savonius type wind turbines can hardly achieve a maximum power coefficient of 0.17. Computational fluid dynamics (CFD) tools are widely used in analysis and simulation of wind turbines. The power output of different wind turbines can be accurately determined using validated CFD analyses. In a study, the effects of different parameters were investigated on power performance of two straight bladed VAWTs. To maximize the power production of each wind turbine, the optimal configuration was obtained and an increase in power generation of nearly 10% was observed [13]. A miniature 4-bladed HAWT was investigated experimentally with and without gear transmission to a generator [14]. The effect of various resistor loads on the performance of the wind turbine generator at wind speeds from 2 m/s to 8 m/s was analyzed. The results indicated that with 20 Ohm resistors, the maximum powers of 106 mW and 126 mW were achieved at a speed of 8 m/s for the micro design without and with gear, respectively [14]. The design of protuberant blades in a small HAWT was optimized both experimentally and numerically to improve the performance of the wind turbine at both low and high rotational speeds [15]. The optimal sinusoidal shape for the blades performed as expected, achieving the maximum power coefficient of about 0.47 for the model without leading edge protuberant [15]. A comprehensive review was conducted on wind power generation through articles from 2005 to 2020 [16]. In this review, the miniaturized HAWTs were classified as those with power generation below 10 kW for individual energy needs in offices, houses, or schools. Various aspects of sustainability in wind power generation were discussed [16]. A novel small impulse 20 bladed HAWT was experimentally and computationally investigated. For the rotor diameter of 30 cm, the maximum power coefficient of 0.17 was obtained at a wind speed of 8.2 m/s generating 4.5 W [17]. The cut-in wind speed of 3.5 m/s was obtained. Economical merits of small wind turbines in urban areas of Germany were evaluated, and it was suggested that positioning of the wind turbines and storage systems are crucial for economic feasibility [18]. The study considered three HAWTs from 2.4 kW to 6.5 kW rated powers. The cut-in wind speed of the selected wind turbines was 2 m/s and 3 m/s and rotor diameter varied from 3 to nearly 13 meters. The payback time of the selected small HAWTs was reported 16 to be 18 years [18]. Long term field testing is an important aspect of assessing small wind turbines that have not received a great deal of attention in the literature. In research on a straight bladed VAWT, the laboratory and field testing were conducted using a torque meter for obtaining the wind turbine torque and different wind measuring devices but without measurements of rotational speeds [19]. The study used a 2 m diameter 2 bladed NACA0021VAWT with 1.2-meter blade length. The rotational speed was not measured nor reported though was claimed as constant. The maximum power coefficient, in both field and wind tunnel testing, was below 0.2 with a cut-in wind speed of 3.4 m/s observed [19].

Two novel counter-rotating 6-bladed VAWTs were integrated and observed to have more than two-fold power generation compared with two single rotor designs. The maximum power of 70 W was obtained at a wind speed of 11 m/s and rotational speed of 240 RPM compared to 30 W for two single rotor designs [20]. The self-starting feature was also claimed to be improved using this H-type Savonius-Darrieus wind turbine design, but the cut-in wind speed of 5 m/s was observed for both single and double rotor designs. The VAWT design included a 0.8 m diameter, 0.5 m height, and NACA0021 type blades. The maximum power coefficient of 0.4 was obtained [20]. One of the deficiencies of small HAWTs is low power performance. The effects of solidity by using three to six blades were investigated on the power performance of small HAWTs [21]. Experimental results indicated that the maximum power coefficient slightly improved by reducing the number of blades from five in the original design to three blades, but the cut-in wind speed increased, which affects the performance of the wind turbine at low wind speeds. Impact of topography and roughness of wind locations on power generation were discussed using various nano to large sizes wind turbines around the world [22]. Wind over buildings was modelled using three inner, middle and outer layers, suggesting accelerated regions like near edges of rooftop buildings are suited for wind power generation. Although highly vortex regions were not recommended for wind power production. For any wind turbine development, a long-term wind assessment from one to ten years with 10 min wind data intervals was recommended [22].

CFD simulation over urban buildings indicated that diffuser enhanced wind turbines performed better at edges of rooftop buildings. The simulation indicated that HAWTs should be located vertically for better output power [23]. The shortcomings of various micro-bladed HAWTs were extensively highlighted with and without various diffuser, shroud, and lens designs, along various blade design strategies [24]. The main issue was observed, the very low power performance of micro power

generation in real life fields. Several recommendations were made including using twisted and tapered blades, paying careful attention to aerofoil shape and dimensions, integrating shrouded diffusers to augment wind power generation up to four-fold, and integrating cost and performance in analyzing new micro wind turbine concepts to achieve high strength to weight ratio [24].

Several curved bladed VAWTs were experimentally investigated [25]. For speeds below 13 m/s the four bladed VAWT performed better whilst for speeds above 13 m/s, the three bladed designs performed better in power generation. The study was too brief to consider the power coefficient versus conventional VAWTs. The design of microgrids HAWTs were re-evaluated using mixed aerofoils in blade design using blade element momentum (BEM) theory and CFD simulations [26]. The results indicated that blade's twist was crucial and mixed aerofoil blade design improved power performance. To tackle the cost of small HAWTs, a simplified manufacturing design of the blade and hub was introduced that reduced the cost of timber blanks and the machining process by 33% and 58%, respectively, for a small 1 kW wind turbine [27]. Although the cost reduction is one of the prime aspects of small wind turbines, the study lacked evaluating power performance and determining payback time. Current challenges on utilizing small HAWTs were investigated in terms of performance, cost, noise, and other factors [28]. One field of research devoted to developing small HAWTs to operate at low wind speeds, which has been facilitated by CFD simulation tools to improve the power coefficient.

In a different work, the concept of a cross-axis wind turbine (CAWT) was integrated in a building and experimentally investigated in a low-speed wind region in Malaysia [29]. The design incorporated three horizontal and three vertical blades. The CAWT design and a straight-bladed VAWT were mounted on a building for comparison. Although the improved design outperformed the conventional VAWT, the maximum power coefficient of 0.1263 was obtained. The cut-in wind speed was not presented for the studied CAWT and VAWT.

Pitch control of small wind turbines is uncommon. However, a cost-effective mechanism may improve designs such as the giant 117-Norwegian offshore wind turbine platform [30]. An experimental work with a pitch control 200 W micro wind turbine in a large wind tunnel with a cross section of $4.0 \text{ m} \times 2.6 \text{ m}$ was performed in Taiwan [31]. A disk pulley mechanism was used to passively control the pitch angle of the wind turbine blades using centrifugal force. At high wind speeds, the pitch control mechanism reduced the rotational speed of the wind turbine, yet such mechanisms need to be optimized [31].

Performance curves of small HAWTs are one of the key factors for power-economy analyses. Power coefficient (C_p) versus tip speed ratio (TSR) should be obtained in any wind turbine development. A fast and reliable method was developed for obtaining performance curves of small HAWTs using a moving cart and measuring the generator voltage [32]. Physics-based mathematical models were used to extract performance curves from the measured values and were validated. A similar technique was developed by accelerating a small wind turbine to determine the wind turbines' power and torque using wind tunnel or field testing [33].

Analyzing new small HAWTs requires a variety of tools from mathematical modelling to CFD simulations and from laboratory testing to field testing. These analyses were performed for a micro 240 W wind turbine using mixed blade aerofoil profiles indicating that the SST k- ω turbulence model in CFD simulation agreed well with the experiment, and the maximum power coefficient value of 0.34 was obtained [34]. A centimeter-scaled micro wind turbine was experimentally tested in a wind tunnel, and power generation was evaluated, as shown by Kim et al. [35], who optimized the rotor diameter—RPM relationship. The 2.6 cm rotor diameter used 8 swirl type blades and tested against various parameters such as resistive loads and yaw angles. The optimal maximum power and the corresponding resistive loads were also identified [35]. The optimal spacing of small HAWTs were experimentally and computationally investigated considering the effects of wind turbines' wakes and particularly the effects of wind turbines' towers [36]. It was found that the Reynolds stress model (RSM) CFD simulation results agreed well with various experimental measurements including hot-wire anemometry, indicating that three-rotor-diameter spacing was the optimal distance between each wind turbines [36].

A review study suggested the Savonius VAWTs as economical and aesthetic micro generation for remote and urban environments and Darrieus rotor type VAWTs as the potential for large-scale wind generation particularly in offshore applications [37].

The variable speed wind turbine (VSWT) is a concept for generating variable frequency electricity that must be controlled to provide a constant frequency to the grid. Various VSWT control methods were reviewed highlighting the limitations of these methods and the need for stabilized frequency [38]. A recent patent review on VAWTs suggested that these wind turbines outperformed conventional HAWTs in unfavourable conditions such as urban environments, trains, low wind speeds, and highly turbulent winds [39]. The study showed a total of 506 patents in VAWT designs of which 64% were produced during the past ten years. Since 2010, sixteen distinct patents were examined thoroughly in the article. Recently, a comprehensive review of origami-inspired systems was presented [40]. The mechanical modelling of foldability and low-energy processes of origami systems was discussed. Additionally, kinematic formulations for reducing the order of models and the nonlinear dynamics of origami systems were examined. Vast applications including architectural designs, robotics, energy harvesting, energy absorbers, biomedical systems, acoustics, and more were explained. The study however did not point out the common windmill origami designs. The design of curved origami theorems and methodology were mathematically explored by Lang [41], whose geometric approach influenced several recent windharvesting concepts. New curved origami designs and appealing patterns were created that could inspire new wind turbine systems. Structural strength of origami designs, referred to as aerogami, were computationally and experimentally investigated in wind tunnel testing [42]. Two composite aerogami designs, namely "worm" and "dino" designs were evaluated for drag force generation. The validated models indicated the usefulness of the designs for implementing in real-world aerodynamic control surfaces [42].

1.2. Focus of the Present Study

The well-known origami paper windmill (or pinwheel) evokes everybody's childhood memories of enjoying the moments of playing with this wind rotating toy. It is so familiar to everyone to even think about how it works. By closely observing the rotation direction and analyzing the wind interaction with the paper windmill, the concept shown in Fig. 1 may be expressing how this toy works.

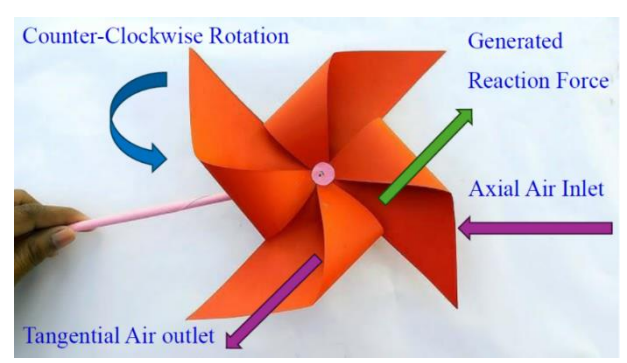


Figure 1. The Origami paper pinwheel (windmill) motion concept.

As shown in Fig. 1, the horizontal wind approaches the face of the origami windmill axially and is captured by its long, flat surfaces. The captured air travels through the tubular section and exits tangentially, generating reaction force. This off-center reaction force produces torque, causing the paper windmill to rotate in a counter-clockwise direction.

1.3. Aesthetics Features of the New Design

Inspired by the origami windmill and knowing most of wind turbines developed to date are either drag or lift operating devices, a novel bladeless and hub less rotor design is introduced that uses neither lift

nor drag. Instead, it uses a reaction force to drive a generator for application in micro wind turbine generations (see in Fig. 2).



Figure 2. The origami inspired rotor design example.

It features a single rotating disk or cylinder that intakes air axially through multiple holes and discharges it tangentially at the outer circumferences. Instead of the drag or lift force, the inspired design uses the reaction force from the mass flow rate leaving the rotor. Based on Newton's second law of motion, the change of momentum will result in a reaction force as illustrated in Fig. 2. The torque developed by the reaction force then directly drives a generator. Eliminating the need for multiple blades and a hub enhances efficiency, reduces noise, and ensures safety for flying wildlife. Additionally, protective nets at the entry and exit of the rotor holes can protect wildlife from entering the disk rotor when it is stationary. The turbine can also be integrated into modern rooftop-edge building designs such as Aeromine [43] or Ventum VX175 [44] or enclosed structures like solar chimneys, providing a quiet and efficient means for generating electricity. The design provides structural stability, reduced noise, and enhanced safety for wildlife. The design can compete with solar power generation in harsh environments that photovoltaic panels may fail due to dust accumulations and soiling issues like in the Gulf Cooperation Council (GCC) countries.

Wind turbine social acceptance has been a persistent subject of controversy. According to Guo and coworkers, "previous research also indicates that wind power projects are unappealing to the local populace if they are built in their neighborhoods because they produce noise and represent unattractive alterations to the landscape" [45]. Petrova [46] highlighted those visual concerns, such as aesthetics and physical characteristics, are among the main reasons for resistance wind turbine installations near residential areas. That has essentially led to the "Not-In-My-Back-Yard" (NIMBY) acronym, which describes opposition to projects within residents' sight and vicinity [46]. In Nordic countries like Denmark and Sweden, several projects have been postponed due to these perceived disadvantages [45].

This paper proposes several design ideas to address these concerns. First, the rotors can be installed as small, compact turbines on rooftop parapets. This configuration minimizes interference with the overall architectural design of the building, as illustrated in Fig. 3.



Figure 3. A rooftop wind turbine and solar energy integration for a building.

Additional design concepts are presented in Fig. 4. Instead of traditional wind turbine towers installed on roof parapets, aesthetically pleasing designs can be implemented on roof terraces. The rotors can be housed within rectangular walls or circular frames, either aligned uniformly or with alternating orientations, providing comprehensive exposure to wind from multiple directions.



Figure 4. Rotors within a rectangular or circular frames.

Fig. 5 illustrates how a sustainable building might appear with the integration of both solar panels and these novel wind turbines, along with electric vehicle (EV) charging points showcasing a holistic approach to renewable energy generation and use in urban environments.



Figure 5. Overall view of a building with renewable energy generation for EV charging.

These design proposals aim to address the aesthetic concerns often associated with wind turbines while maintaining their functionality and efficiency in utilizing wind energy within urban settings.

1.5. Limitations of the Current Design

Scaling up to small HAWTs of kW-powered sizes requires larger diameters that proportionally increase the width of rotor and add to its weight. Another potential issue is the thrust force on the mast of wind turbine that needs to be structurally assessed; although the dynamic load will be different on the mast compared with blade-type HAWTs. The cut-in wind speed needs to be improved so that the rotor design can operate effectively at low wind speed regions. Further research is needed to optimize the design of the proposed single rotor for larger applications.

1.6. Outline of the Paper

The paper presents a novel wind rotor design inspired by the origami paper windmill. The section presents a recent literature on developments of micro wind turbine concepts from various distinct VAWTs designs to limited HAWTs research and introduces the origami designs to inspire micro scale

HAWTs developments. Also, this section presents the aesthetic features of the new rotor design for integration in buildings. Section 2 deals with materials and presents 3D print models, mechanical components, the generator used, wind tunnel, and measurement equipment. The mathematical modelling and experimental approach are also discussed. Section 3 provides 3D printed models, experimental results with/without generator and load. Section 4 summarizes the findings of this research and draws conclusions.

2. MATERIALS AND METHODS

2.1. 3D Prints

The FlashForge with dual extruder 3D Printer was used to produce 3D prints of the rotor models investigated here [47]. The highest temperature of the extruder is $300\,^{\circ}$ C. The maximum printable dimension is $300\,\text{mm} \times 250\,\text{mm} \times 200\,\text{mm}$. The print speeds vary from 10 to $150\,\text{mm/s}$ with an extruder diameter of $0.4\,\text{mm}$. 3D prints can be produced under three categories: Fast, standard, and fine. For successful printing, the following settings were used: The standard option with, an extruder temperature of $190\,^{\circ}$ C, and a platform temperature of $50\,^{\circ}$ C. The printer's cooling fan was set to zero speed for the initial 5 layers and to 25% cooling speed from layer 6 onwards. The supporting layer option was also enabled. Each model took between 5 and 30 hours to print. Fig. 6 shows one of the rotor designs, which was 3D printed in 12 hours.



Figure 6. The origami inspired rotor design 3D print example.

2.2. Mechanical Components

Figs. 7(a,b) show the standard mechanical holder for testing the free rotation of the rotor in two views. A 3/8-inch (9.525mm) steel tube with an outer diameter (OD) of 9.525 mm was inserted in the central hole (size of 10 mm) of the rotor design allowing it to rotate freely under the effects of wind. Two small ball bearings were located before and after the rotor to guard the rotor against axial movement. The bearings were held in place by two cotter pins.

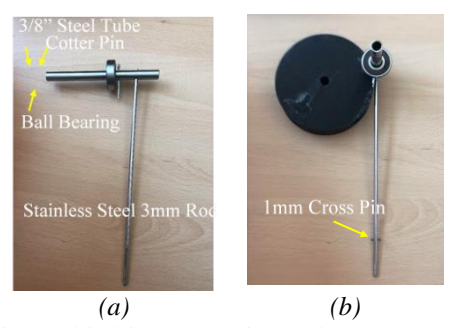


Figure 7. The rotor mechanical holder for wind tunnel testing: (a) Side view, (b) axial view

Figs. 8(a,b) show the fabricated mechanical holder for testing the generator connected with the rotor. A stainless-steel bar of 4 mm diameter with a standard length of 210 mm was fixed vertically and a tube with a cross pin of 1mm diameter at 25 mm lower part for insertion in the wind tunnel strain gauge balance system.

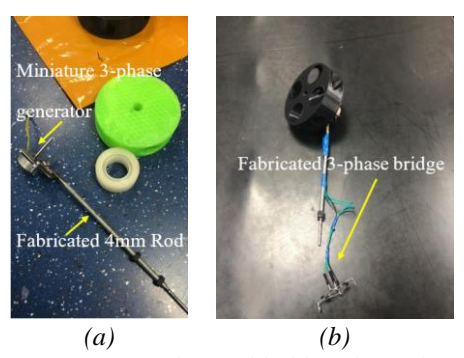


Figure 8. The fabricated components: (a) Mechanical holder, (b) 3-phase micro generator components.

2.3. Three-Phase Micro Generator

A three-phase generator was used with the aid of a bridge rectifier (see Figs. 8(a,b)), to efficiently and reliably generate and convert power from AC to DC. A three-phase system is more efficient for producing power with less fluctuation than a single-phase system, making the output smooth and even. The three-phase systems produce less harmonic distortion, which means smooth DC output, and they can handle higher power levels with balanced load distribution.

This is a very important feature to maximize energy harvesting particularly at micro scales. The basic rectification is crucial for converting the three-phase AC into stable DC. As shown in Fig. 9, a bridge rectifier, composed of six diodes connected in series and parallel within the circuit, is used to convert AC into DC for charging batteries or powering common DC applications in off-grid or hybrid setups.

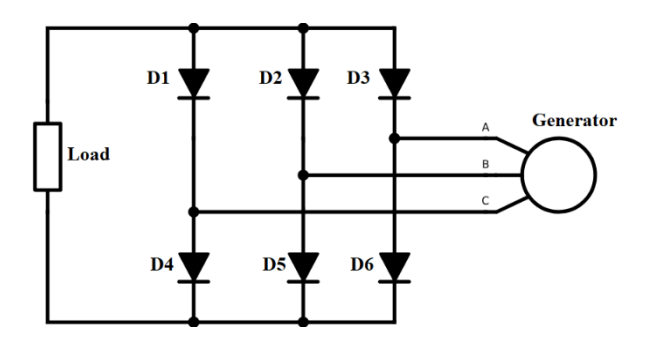


Figure 9. Three phase bridge rectifier circuit.

The miniature brushless 3-phase generator was used to measure the output power of the rotor designs. This variable speed generator can produce an AC voltage range of 3-24V for the studied wind turbine rotors. The three-phase generator design provides smooth and efficient operation for a variety of DIY project models and useful for educational purposes. The tiny size and very light structure of the miniature generator make it a convenient tool for wind tunnel testing. The maximum output power is 12 W with a current rating of 1 A and a frequency of 50 Hz. Its dimension is 29.97 mm (L) × 28.45 mm (W) × 29.97 mm and 79.93 grams weight (see Fig. 9). This generator is made of durable metal material.

2.4. The Tachometer

AGPtek® professional digital laser photo tachometer was used to measure the rotational speed of the wind turbine rotor (see in Fig. 10). The device can measure rotational speed in a range from 2.5 rpm to 99999 rpm with a resolution of 1 rpm.

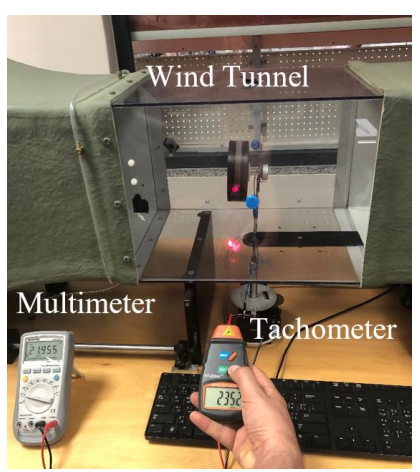


Figure 10. The wind tunnel tests the wind turbine rotor using a tachometer and a multimeter.

The tachometer can measure rotational speeds of any rotating object within a detecting distance range of 50 mm to 500 mm using a 9V battery. The operating temperature is $0 \sim 50$ °C, the dimensions are 131 (*L*) x 70 (*W*) x 29 (*D*) mm, and the weight is 160 g. By applying a reflective mark on a rotating object and aiming at the mark by the laser beam, the rotational speed is displayed with five digits on the 18 mm LCD display. The sampling time is 0.8 seconds.

2.5. The Multimeter

As shown in Fig. 10, the GW Instek GDM-397 multimeter was used in this experiment to measure the output voltage of the 3-phase generator. It is a handheld digital multi-meter with the following specifications: 3 3/4 digits, 3999 counts, DC/AC voltage (up to 1000 V/750 V), DC/AC current (up to 10 A), resistance (up to 40 M Ω), capacitance (up to 4000 μ F), frequency (up to 10 MHz), diode test, continuity, temperature measurement, duty cycle. DC voltage accuracy is \pm (0.5% + 1 digit), and AC voltage accuracy is \pm (1.0% + 3 digits).

The rotor was directly coupled to a small three-phase micro generator, and output voltage and current were measured using a digital multimeter (UNI-T UT61E) at the generator terminals. Power was calculated as the product of measured voltage and current under resistive load conditions. For constant-load tests, a $1.5~\Omega$ resistor was used as the load, and values were logged manually at each wind speed increment. Measurements were repeated three times to ensure repeatability, and average values were used for reporting.

2.6. The Wind Tunnel

The wind tunnel in this work is the HM 170 GUNT model [48] (see in Fig. 10), which is an "Eiffel" type open wind tunnel for testing small model sizes within its square test section size of 292 mm (W) × 292 mm (W) and the length of 420 mm (W). The air is drawn in from the inlet nozzle accelerated through a honeycomb mesh inlet passes through a transparent test section and then decelerated in a diffuser section and pump out by the fan and its 3.4 kW motor (with typical 230 V, 50 Hz, single phase) of the wind tunnel at the back. The full dimensions of the wind tunnel are 2870 mm (W) × 1540 mm (W) with total weight of 250 kg.

The carefully designed nozzle profile and the flow straightener honeycomb ensure a uniform velocity with little turbulence in the test section. Air speeds from 1.3 m/s and up to 25 m/s can be reached in this open wind tunnel. The wind tunnel is equipped with a balance system to measure and display lift and drag forces of up to 4 N and within $\pm 180^{\circ}$. The air speed in the test section is measured using the inclined tube manometer. All measured values of air speed, lift and drag forces, moment, displacements and angles and the differential pressures are processed by a data acquisition system and displayed on a personnel computer (PC) using the designated software [48].

3. THEORETICAL APPROACH

The linear momentum equation obtained by Newton's second law of motion is expressed for a fixed control volume as follows [49]:

$$\sum \vec{F} = \frac{d}{dt} \left(\int \rho \vec{V} dV \right)_{CV} + \left(\int \rho \vec{V} (\vec{V} \cdot \vec{n}) dA \right)_{CS}$$
 (1)

In Eq. (1), $\sum \vec{F}$ is the sum of all external forces, the first integral in the right is the time rate of change of linear momentum of the contents of the control volume (CV), and the second integral is the net flow rate of the linear momentum out of the control surface (CS) by the mass flow rate. In the integrals in Eq. (1), ρ is density of air, \vec{V} is the velocity vector, $d\vec{V}$ is the differential volume, dA is the differential area, and \vec{n} is the normal unit vector perpendicular to the CS. Considering a fixed control volume (CV) around the wind turbine and assuming wind is normal to the control surface at the inlet (in axial direction) and at the outlet (in tangential direction) and the entire control surface (CS) is at atmospheric pressure, then the Eq. (1) for the steady two-dimensional flow is obtained as follows [49]:

$$F_a = \dot{m}V_{in} \quad [N]$$

$$F_t = \dot{m}V_{out} \quad [N]$$
(2)

In Eq. (2), F_a is the axial force or the unfavourable thrust or drag force that must be minimized, however, F_t is the favourable reaction force. A torque is generated by tangential force multiplied by the rotor radius and the wind turbine power is generated by the torque multiplied by the rotational speed of the rotor. Hence, the tangential force must be maximized to obtain maximum output power. The mass flow rate is defined by $\dot{m} = \rho A_{out} V_{out}$, expressing the amount of air that get into the rotor and leaves through the outlet.

An experimental study on external flows around nozzles, tubular section, and diffusers indicated that the free stream velocity is retarded at the inlet of nozzles (V_{in} is smaller than V_{out}) and regain its magnitude at the outlet ($V_{out} = V$), which is equals to the freestream wind velocity (V) [50].

For diffuser designs, it was opposite, wind speed was accelerated at the inlet and reduced to the wind speed, V, at the outlet. For tubular section, the measurement indicated that the inlet and outlet velocities remained equal to the freestream wind speed.

For the new rotor design with internal elbow shape 3D nozzles, a correcting factor, β , is introduced to account for energy loss and turbulence on entry and exit of the 3D nozzle conduits. Hence, the outlet velocity is corrected by the β factor (i.e., $V_{out} = \beta V$).

To decrease the magnitude of the axial force, F_a , the inlet velocity, V_{in} , must be reduced by incorporating a nozzle within the new rotor design. Hence, the aspect ratio of the nozzle is defined by [49]:

$$AR = \frac{A_{in}}{A_{out}} \tag{3}$$

Higher values of the aspect ratio AR, has advantageous of smaller V_{in} and consequently smaller F_a , and smaller width of the rotor. But it is at the cost of decreasing outlet area A_{out} and consequently reducing the mass flow rate \dot{m} . The torque and power of rotor with the radius R is calculated as follows [49]:

$$T_R = F_a R [Nm]$$

$$P_R = T_R \omega [W]$$
(4)

In Eq. (4), T_R is the torque, P_R the output power of rotor, and ω is the angular velocity in rad/s. The power coefficient can be calculated using the wind power for the rotor with the radius R and the rotor area $A_R = \pi R^2$, as follows [50]:

$$P_W = \frac{1}{2}\rho A_R V^3 \quad [W]$$

$$C_P = \frac{P_R}{P_W} \tag{5}$$

In Eq. (5), P_W is the wind power, ρ the air density, V is the wind speed, and C_P is the power coefficient. The tip speed ratio (TSR) is determined by [50]:

$$\lambda = TSR = \frac{R \ \omega}{V} \tag{6}$$

The performance of wind turbines is usually expressed by $C_P - \lambda$ performance curves.

3.1. Model Limitations and Future Refinement

The present theoretical analysis adopts idealized assumptions such as purely tangential airflow and a constant correction factor β across different aspect ratios. While these approximations simplify the mathematical formulation and allow for initial performance estimation, they may not fully represent real-world flow behavior - especially in complex urban wind environments where turbulence, angular inflow, and recirculation effects are common. Future improvements to the model may incorporate experimentally derived or CFD- calibrated β values that account for changes in Reynolds number (Re), flow angle, and rotor geometry. Additionally, extending the analysis to include partial radial inflow components and dynamic stall phenomena could enhance the predictive accuracy of the model, particularly at low wind speeds or during gusty conditions.

4. RESULTS

4.1. Theoretical Results

Based on the mathematical modelling discussed in Section 3, it is assumed that the air outlet from the rotor is completely in the tangential direction. Using the aspect ratio values of AR = 1, 2, 3, and the correcting factor values of $\beta = 0.1, 0.2, 0.3$, it is assumed that for every 1 m/s wind speed, the rotor rotates at 100 rpm increment. The theoretical results for the expected output power and normal force of the rotor design are shown in Figs. 11(a,b). Experimental values for Models 5 and 6 are also compared with the theoretical values.

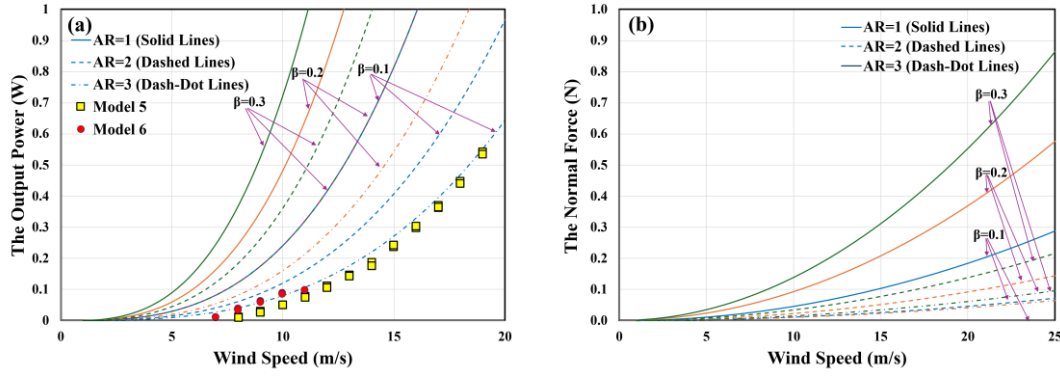


Figure 11. Theoretical performance of the new rotor wind turbine: (a) The output power performance, and (b) the normal force values, at different nozzle aspect ratios and correcting factors.

4.2. Benchmarking against Conventional Small Wind Turbines

To contextualize the performance of the origami rotor, it is valuable to benchmark its output against conventional small HAWTs and VAWTs commonly deployed in low-speed urban applications. Reported power coefficients (C_p) for traditional micro-HAWTs typically range between 0.25 and 0.35 under ideal conditions, while VAWTs often achieve C_p values between 0.15 and 0.25, depending on geometry and wind profile. In comparison, the origami-inspired rotor in this study demonstrates a peak C_p of approximately 0.14 in the best-performing AR configuration. While this is modest relative to conventional systems, the origami rotor offers several compensating advantages. Most notably, the design achieves a significantly lower cut-in wind speed (\sim 2.2 m/s), making it suitable for low-wind urban environments where conventional turbines remain inactive. Additionally, the compact, bladeless, and hubless architecture improves safety, reduces acoustic noise, and enhances visual integration- key factors in urban social acceptance. The ability to 3D print the rotor using low-cost materials also contributes to its scalability and manufacturability, offering a compelling alternative in distributed energy scenarios where aesthetics, noise, and modularity are prioritized over peak aerodynamic efficiency.

4.3. Economic Considerations

Although the current design is at the proof-of-concept stage, a preliminary economic assessment was conducted to compare its feasibility relative to conventional micro-turbines. The origami-inspired rotor benefits from simplified geometry and the potential for rapid, low-cost manufacturing using 3D printing or moulded thermoplastics. Estimated material costs for a full-scale unit remain under 20 Kuwaiti Dinars (\approx 65 USD), significantly lower than commercial micro-HAWTs with comparable dimensions.

Maintenance requirements are also expected to be minimal due to the bladeless, hubless nature of the design, which reduces wear-prone moving parts. This structural simplicity may result in extended operational lifespans and lower servicing costs. While the current power output remains modest, the design's ability to operate at lower wind speeds improves its overall energy harvesting potential in urban environments. Future iterations integrated with low-friction generators may yield higher capacity factors, leading to improved return on investment (ROI), especially in areas with limited solar access or where rooftop space is shared. A detailed life-cycle cost analysis will be pursued following field testing and scale-up validation.

4.4. The Studied Rotor Models

Several models of the single wind turbine rotor were 3D printed with a variety of aspect ratio values to investigate at what AR the rotor these performs efficiently. These models were tested in the wind tunnel. Summary of specification of these rotors are provided in Table 1.

Table 1. Specification of the studied origami inspired rotor designs.

Model no.	Model shape	Specification	Comments
Model 1		Length: 20 cm Diameter: 10 cm Inlet nozzle diameter: 3.5 cm Outlet nozzle diameter: 0.5 cm Aspect Ratio (AR): 49	The rotor failed to rotate at maximum wind tunnel speed of 25 m/s.
Model 2	6	Length: 3 cm Diameter: 10 cm Inlet nozzle diameter: 3.5 cm Outlet nozzle diameter: 0.5 cm Aspect Ratio (AR): 49	The rotor failed to rotate below the wind tunnel speed of 20 m/s.
Model 3	3	Length: 3 cm Diameter: 10 cm Inlet nozzle diameter: 3.5 cm Outlet nozzle diameter: 1.0 cm Aspect Ratio (AR): 12.25	The rotor failed to rotate below the wind tunnel speed of 18 m/s.

Model 4	Length: 3 cm Diameter: 10 cm Inlet nozzle diameter: 3.5 cm Outlet nozzle diameter: 1.5 cm Aspect Ratio (AR): 5.4	The rotor failed to rotate below the wind tunnel speed of 15 m/s.
Model 5	Length: 3 cm Diameter: 10 cm Inlet nozzle diameter: 3.5 cm Outlet nozzle diameter: 2.0 cm Aspect Ratio (AR): 3.0	The rotor starts rotating at wind tunnel speed of 3 m/s.
Model 6	Length: 3 cm Diameter: 11 cm Inlet nozzle diameter: 3.5 cm Outlet nozzle diameter: 2.5 cm Aspect Ratio (AR): 1.96	The rotor starts rotating at wind tunnel speed of 3.4 m/s.
Model 7	Length: 6 cm Diameter: 20 cm Inlet nozzle diameter: 7 cm Outlet nozzle diameter: 5 cm Aspect Ratio (AR): 1.96	The rotor was printed 90% incomplete but starts rotating at wind tunnel speed of 2 m/s.

4.5. Experimental Results for Scenario 1: Without Generator

The models described in Table 1 were tested in wind tunnel. Only models 5, 6, and 7 were performed to acceptable level. For the larger 20 cm model 7, the wind tunnel test was carried out below 10 m/s due to limitation of model size in the wind tunnel to avoid any damage to the balance system. Fig. 12 compares these three models without a generator.

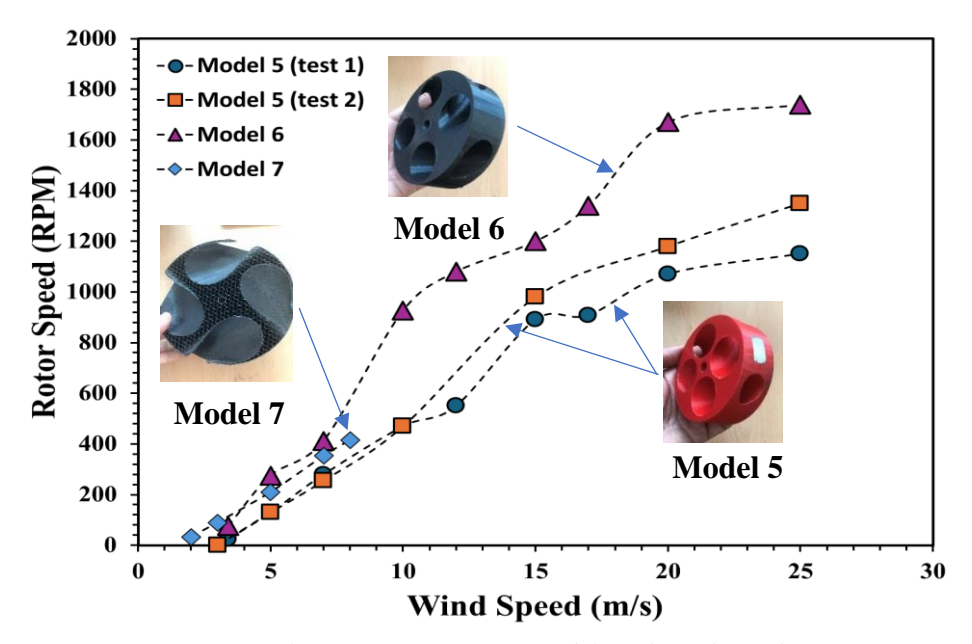


Figure 12. Experimental performance of rotor models without the 3-phase generator.

4.6. Experimental Results for Scenario 2: With Generator

In testing with the 3-phase generator, a fresh 3D print of model 5 and model 6 were tested in wind tunnel and rotor speed and voltage of the generator were recorded as illustrated in Figs. 13 and 14.

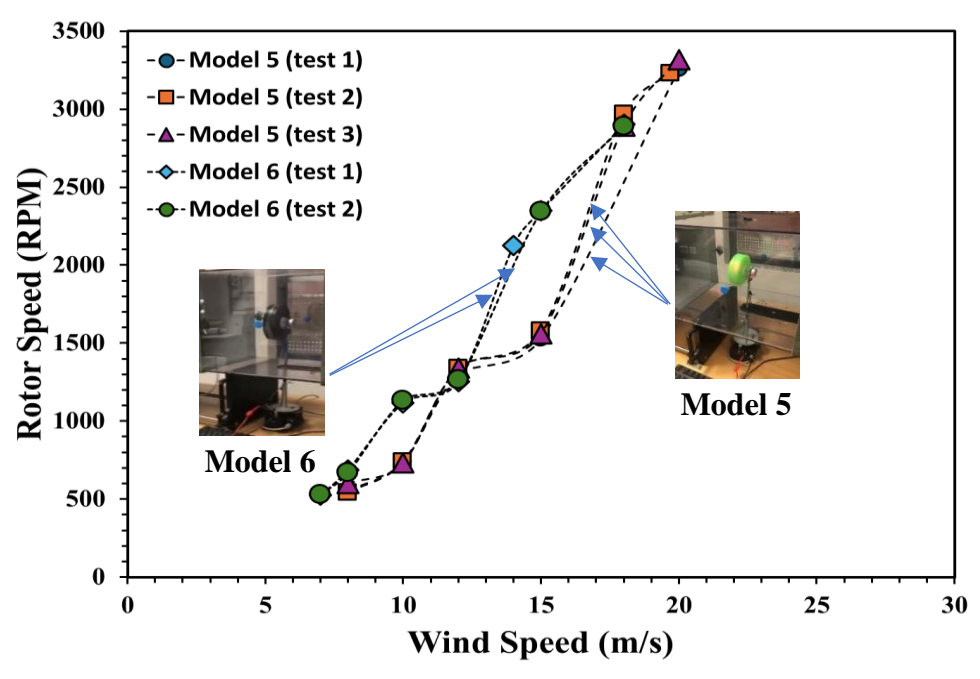


Figure 13. Experimental performance of the rotor speed for models 5 and 6 with the 3-phase generator.

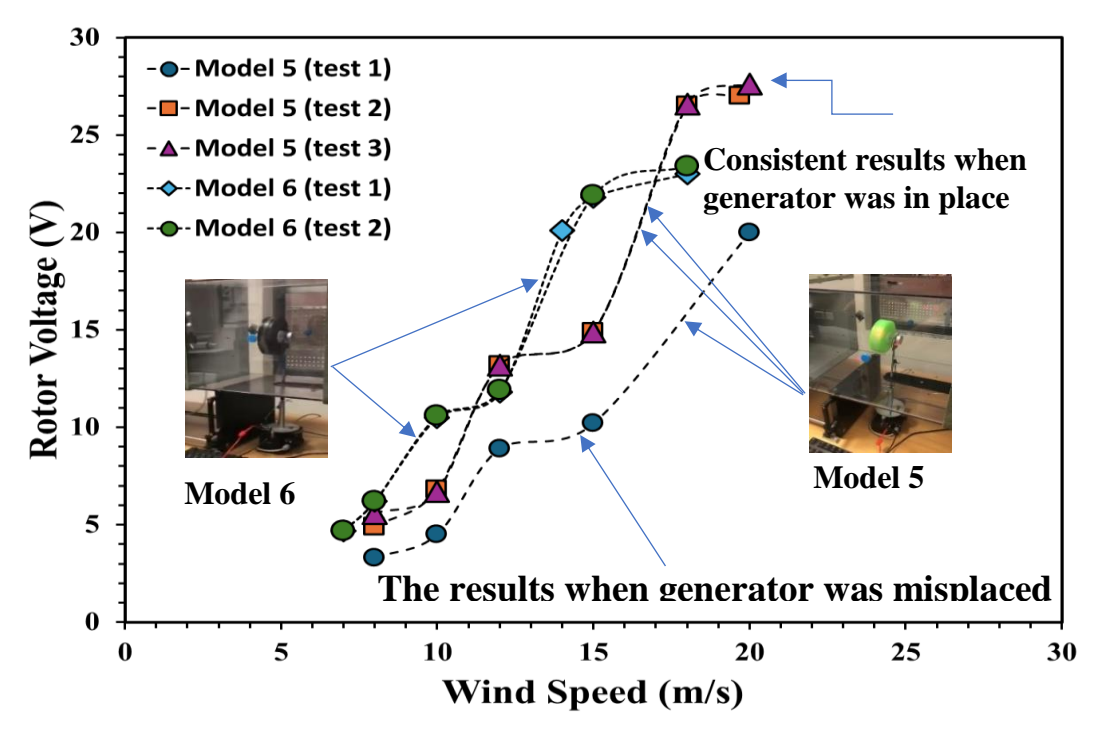


Figure 14. Experimental performance of the rotor voltage for models 5 and 6 with the 3-phase generator.

4.7. Experimental Results for Scenario 3: With both Generator and Load

Models 5 and 6 were tested in the wind tunnel. Model 6 exhibit unbalances lead to vibrations above 11 m/s but the smaller model 6 performed well up to wind speed of 19 m/s. The output of the 3-phase generator was connected to a low current LED bulb and output power was measured using two multimeters to measure voltage and current. Each model was tested three times from wind speeds from 7 m/s to 19 m/s. The output power for the two models is compared in Fig. 15.

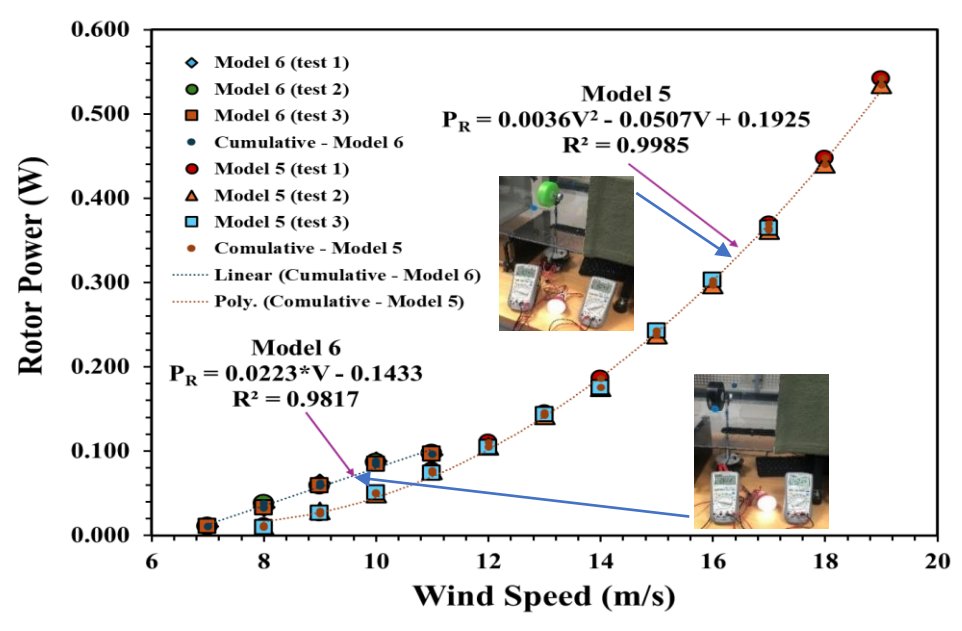


Figure 15. Experimental power performance of the rotor models 5 and 6 with the 3-phase generator and load.

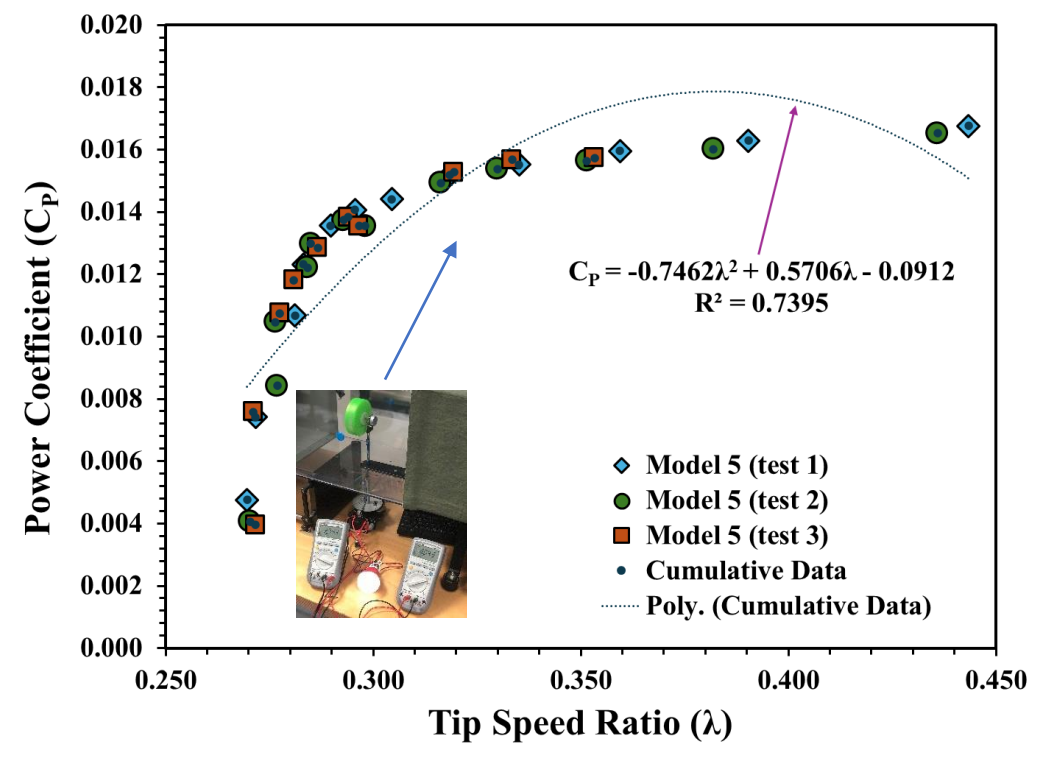


Figure 16. Experimental power coefficient as the function of tip speed ratio for rotor model 5.

5. DISCUSSION

5.1. Discussion on Theoretical Results

For the theoretical results, the dimensions of the rotor design and nozzle holes are assumed as follows: the rotor diameter is 10 cm and each of inlet diameters is of 3.5 cm. As observed in Fig. 11, for the

AR = 1, the maximum output power and normal force are obtained as 3.78 W and 2.9 N, respectively. These values are reduced to 1.89 W and 0.72 N for the AR = 2, and 1.26 W and 0.32 N for the AR = 3. Based on the above theoretical assumptions, the constant power coefficients values of 0.0513, 0.0257, and 0.0171 are obtained for AR = 1, 2, 3, respectively, at all tip speed ratio values of $\lambda = 0.0524 \cdots 1.31$.

5.2. Discussion on Experimental 3D Print Models

The wind tunnel testing was conducted under three scenarios. In the first scenario, the rotor was mounted on the shaft design described in Fig. 3 to ascertain load free rotation of the models. Some of these models failed to rotate or only started rotating at very high wind speeds. In the second scenario, the well performed models were selected and connected to the 3-phase generator without a load as illustrated in Fig. 8. The performance of these models to create output voltage then were assessed. In scenario three, the selected models were connected to the 3-phase generator and a low current electric LED bulb load.

As illustrated in Table 1, the models with the nozzle AR above 3 failed to rotate effectively. Decreasing the nozzle AR to 3 and 1.96 improved the rotor design operation. With lower AR of 1.96, the rotor run faster than AR of 3 but no noticeable improvements in the cut-in wind speeds. Increasing the rotor size from 10 cm diameter to 20 cm diameter improved the cut-in speed from 3 m/s to 2 m/s. The findings in Table 1 indicate that the rotor design can be improved by optimizing the shape and size to an effective and highly efficient rotor in micro wind turbine applications.

5.3. Discussion of Results for Scenario 1

As observed in Fig. 12, the behavior of the studied rotor speeds is nearly linearly dependent to the wind speeds. Model 6 has the highest rotor speeds and Model 7 has the lowest cut-in wind speed although this model is not fully 3D printed. The results for Model 7 are illustrated here to show that even open origami rotor designs such as those shown in Fig.1 are viable options for exploring new HAWT rotor designs.

5.4. Discussion of Results for Scenario 2

As observed in Fig. 13, the model 6 performed better at lower wind speeds below 15 m/s and rotor speed are higher than the model 5. As illustrated in Figs. 13 and 14, the repeatability of the results is confirmed for the model 5 using three test runs, and two test runs for model 6. In the first test run for model 5, we noticed the generator produced lower voltage because of stator had slightly misplaced due to wind speed. By fixing this issue, the second and third runs showed consistent results for voltage as illustrated in Fig. 13. As observed in Figs. 13 and 14, the cut-in wind speed for model 6 was slightly better with the value of 7 m/s in comparison with the model 5 with the value of 8 m/s. The cut-in wind speed feature of these rotors needs to be improved.

Fig. 14 compares voltage of the 3-phase generator at different wind speeds using the rotor models 5 and 6. The model 6 has performed better than model 5 at wind speeds below 15 m/s generating higher voltage. This suggest that the rotor with lower aspect ratio (AR) of 1.96 can perform better at lower wind speeds.

5.5. Discussion of Results for Scenario 3

Fig. 15 shows the output power results for both models in three tests run and their linear and second-order polynomial fit functions have adequately fitted the data with *R*-squared above 0.98. Model 6 started producing electricity at the wind speed of 7 m/s and Model 5 at the wind speed of 8 m/s. Model 6 has better output power and Model 5 has produced consistently at all wind speeds to the maximum output power of 0.542 W at the wind speed of 19 m/s.

Fig. 16 presents the power coefficient of the micro rotor model 5 against tip speed ratios. The maximum power coefficient (C_P) of 0.0168 was obtained at the tip speed ratio (TSR) of 0.4434. Small wind turbines should operate at their optimal TSR of 6 to 8 while the larger wind turbine will operate effectively at TSR values between 8 to 10. More improvements are required on the design of the new rotor before enlarging it to small wind turbine sizes.

5.6. Scaling and Durability Considerations

While the current study focused on small-scale 3D-printed rotor prototypes, scaling the origami-inspired design to practical sizes for rooftop or commercial deployment raises important structural and material considerations. The durability of fold lines, resistance to fatigue under cyclic loading, and material degradation due to UV exposure or moisture must be addressed in future studies. Suitable materials for long-term outdoor exposure, such as UV-stabilized thermoplastics, aluminum composites, or fiber-reinforced polymers, should be evaluated. Additionally, structural simulations incorporating gust response and vibrational behavior will be essential for predicting long-term mechanical performance. Fatigue testing under simulated urban wind turbulence can further help validate the reliability of the system for continuous operation in real-world conditions.

5.7. Planned Field Testing in Urban Environments

While the present study is limited to controlled wind tunnel experiments, we recognize the importance of validating the rotor's performance under real-world urban conditions. Field testing is planned as a critical next step to assess operation in naturally turbulent, low-speed, and multidirectional wind environments commonly encountered in cities. Such testing will enable evaluation of startup behaviour, directional responsiveness, and power stability over extended periods, and will inform necessary design adaptations for rooftop or facade-mounted deployment.

In addition to the performance and structural benefits of the proposed bladeless rotor design, environmental sustainability has been a core consideration in its development. The design's slow-rotating and bladeless architecture minimizes risks to birds and bats, unlike conventional bladed turbines known to cause significant wildlife fatalities. Protective mesh screens at air entry and exit points further enhance wildlife safety during both operation and idle conditions.

From a sustainability perspective, the rotor structure is designed for recyclability, with potential to be fabricated using thermoplastics, bio composites, or other low-impact materials. Moreover, due to its geometrical simplicity and absence of complex blade aerodynamics, the manufacturing process can be optimized to reduce material waste and embedded carbon, making it more compatible with low-carbon production methods such as additive manufacturing. These attributes position the design as both functionally effective and environmentally responsible, particularly for urban and rooftop deployment where ecological sensitivity and public acceptance are critical.

6. CONCLUSION

An inspired origami bladeless and hub less new wind turbine designs were devised with a single rotating disk or cylinder. Being a single rotor micro wind energy generator has many advantageous in comparison with the typical bladed micro designs including better power performance, decreasing noise levels, eliminating hub and blades, integrating capabilities with buildings, being aesthetics for building integration, and being safe to wildlife birds. The rotor intake receives axially air flow and discharges tangentially through several tubular conducts to create a reaction force. The concept of using reaction force by changing the direction of mass flow rate and momentum of air flow is new in wind turbine designs. Various nozzle aspect ratios for the tubular conducts were manufactured using 3D prints. Seven

models of the rotor designs were investigated in a subsonic wind tunnel at Australian University (AU), Kuwait.

Three scenarios were investigated. In the first scenario, the rotor designs were allowed to rotate freely under the effect of wind speed in the wind tunnel. In the second scenario, the rotor designs were connected to the three-phase micro generator and electricity generation were evaluated. In the third scenario, the power generation was evaluated using a constant load in wind tunnel tests. The following conclusions are drawn:

- Out of seven models, only three models were successfully performed under the effects of wind speed in the wind tunnel testing.
- With the nozzle AR lower than 3, the four tubular sections within the origami design has facilitated air flow under testing in the wind tunnel.
- In the first scenario, the Model 6 with the AR of 1.96 was performed better and started at the cut-in wind speed of 3.4 m/s and attained the rotor speed of 1740 rpm at the wind speed of 25 m/s. Both Model 5 and Model 6 started at the cut-in speed of 3.4 m/s at idle rotation. However, by increasing the rotor diameter from 10cm to 20cm in Model 7, the cut-in wind speed had been improved from 3.4 m/s to 2 m/s in idle rotation.
- In the second scenario, by directly connecting the rotors to the three-phase micro generator, Model 6 reached to a maximum 2900 rpm and 23.2 volt at the wind tunnel air speed of 18 m/s. Model 5 reached to an average maximum speed of 3268 rpm and 27.3 volt at an air speed of 20 m/s. The cutin wind speed was increased to the values of 7 m/s and 8m/s for Model 6 and Model 5, respectively, when these were connected to the three-phase generator.
- In the third scenario, Model 6 outperformed Model 5 up to the air speed of 11 m/s, achieving a maximum power of 0.097 W at this speed. Model 5 obtained the maximum power of 0.365 W at the air speed of 17 m/s. This model obtained a maximum average power coefficient of 0.0158 at an average tip speed ratio of 0.355 at the air speed of 17 m/s. Comparable studies on micro-scale Darrieus turbines reported Cp values in the range of 0.02–0.04 under similar Reynolds number conditions [47,48], positioning the current design within the expected micro-scale performance envelope.

This work serves as a proof of concept, focusing on enhancing the design of origami rotors for improved start-up capability at lower cut-in wind speeds and increasing the efficiency. Future work will involve long-term field testing of optimized rotors, benchmarking against conventional micro HAWTs and VAWTs of comparable size, and further refinement of geometry to enhance power output and reduce material usage. Similar efficiency studies with alternative horizontal and vertical small wind turbine designs have been added in the literature review for comparison. Moreover, enlarged rotor configurations will be tested in real-world conditions to compare an optimized origami wind turbine versus a conventional bladed micro wind turbine.

Acknowledgement

We wish to acknowledge the support of all the staff at the Australian University (AU) of Kuwait. Their help and advice were highly appreciated.

We wish to acknowledge Mr. Girish Kaimal Mohanan from the Fluid Mechanics Laboratory for processing all 3D prints. We are also grateful to Mr. Waqar Jan Zafar from the Electrical and Electronics laboratory for assisting in assembling rotors to the generator and helping with power measurements. We also gratefully wish to thank the engineers and technicians at the AU workshop, particularly Mr. Subramaniam Sundaram, Mr. Hamid Heidar Saadi, and Mr. Joshith Valiyaparambath, and other workshop members, for their help in manufacturing the mechanical stands for wind tunnel testing. Finally, we are indebted to Dr. Ehab Bani Hani for allowing us to use the 3D printer from the PBL (Project-Based Learning) center.

REFERENCES

- [1] Chong WT, Muzammil WK, Wong KH, Wang CT, Gwani M, Chu YJ, Poh SC. Cross axis wind turbine: Pushing the limit of wind turbine technology with complementary design. *Appl Energy* 2017; 207: 78–95.
- [2] Thoppil A, Akbar AA, Rambabu D. Dynamic analysis of a tri-floater with vertical axis wind turbine supported at its centroid. *Journal of Energy Systems* 2021; *5*(1): 10–19. DOI: 10.30521/jes.811097.
- [3] Sunderland K, Woolmington T, Blackledge J, Conlon M. Small wind turbines in turbulent (urban) environments: A consideration of normal and Weibull distributions for power prediction. *J Wind Eng Ind Aerodyn* 2013; *121*: 70–81.
- [4] Scappatici L, Bartolini N, Castellani F, Astolfi D, Garinei A, Pennicchi M. Optimizing the design of horizontal-axis small wind turbines: From the laboratory to market. *J Wind Eng Ind Aerodyn* 2016; *154*: 58–68.
- [5] Jafari SAH, Kwok KC, Safaei F, Kosasih B, Zhao M. The effects of installation configuration and solidity on the power generation of a linear cascade wind turbine. *J Wind Eng Ind Aerodyn* 2018; *180*: 122–135.
- [6] Vaz JR, Wood DH. Aerodynamic optimization of the blades of diffuser-augmented wind turbines. *Energy Convers Manag* 2016; *123*: 35–45.
- [7] Limacher EJ, da Silva PO, Barbosa PE, Vaz JR. Large exit flanges in diffuser-augmented turbines lead to sub-optimal performance. *J Wind Eng Ind Aerodyn* 2020; 204: 104228.
- [8] Scungio M, Arpino F, Focanti V, Profili M, Rotondi M. Wind tunnel testing of scaled models of a newly developed Darrieus-style vertical axis wind turbine with auxiliary straight blades. *Energy Convers Manag* 2016; *130*: 60–70.
- [9] Fertahi SD, Rehman S, Benini E, Lahrech K, Samaouali A, Arbaoui A, Kadiri I, Agounoun R. Insights from the last decade in computational fluid dynamics (CFD) design and performance enhancement of Darrieus wind turbines. *Processes* 2025; *13*: 370. DOI: 10.3390/pr13020370.
- [10] Xu Z, Feng YH, Zhao CY, Huo YL, Li S, Hu XJ, Zhong YJ. Experimental and numerical investigation on aerodynamic performance of a novel disc-shaped wind rotor for the small-scale wind turbine. *Energy Convers Manag* 2018; *175*: 173–191.
- [11] Ma C, Wang G, Wang D, Peng X, Yang Y, Liu X, Yang C, Chen J. Optimization design and performance analysis of a bio-inspired fish-tail vertical axis wind rotor. *Energy Convers Manag* 2024; 300: 117901.
- [12] Antar E, Elkhoury M. Parametric sizing optimization process of a casing for a Savonius vertical axis wind turbine. *Renew Energy* 2019; *136*: 127–138.
- [13] Chen WH, Chen CY, Huang CY, Hwang CJ. Power output analysis and optimization of two straight-bladed vertical-axis wind turbines. *Appl Energy* 2017; *185*: 223–232.
- [14] Xu FJ, Yuan FG, Hu JZ, Qiu YP. Miniature horizontal axis wind turbine system for multipurpose application. *Energy* 2014; 75: 216–224.
- [15] Huang CC, Bai CJ, Shiah YC, Chen YJ. Optimal design of protuberant blades for small variable-speed horizontal axis wind turbine—experiments and simulations. *Energy* 2016; *115*: 1156–1167.
- [16] Azam A, Ahmed A, Wang H, Wang Y, Zhang Z. Knowledge structure and research progress in wind power generation (WPG) from 2005 to 2020 using CiteSpace based scientometric analysis. *J Clean Prod* 2021; 295: 126496.
- [17] Ying P, Chen YK, Xu YG. An aerodynamic analysis of a novel small wind turbine based on impulse turbine principles. *Renew Energy* 2015; 75: 37–43.
- [18] Grieser B, Sunak Y, Madlener R. Economics of small wind turbines in urban settings: An empirical investigation for Germany. *Renew Energy* 2015; 78: 334–350.
- [19] Maeda T, Kamada Y, Murata J, Yamamoto M, Ogasawara T, Shimizu K, Kogaki T. Study on power performance for straight-bladed vertical axis wind turbine by field and wind tunnel test. *Renew Energy* 2016; 90: 291–300.
- [20] Didane DH, Rosly N, Zulkafli MF, Shamsudin SS. Performance evaluation of a novel vertical axis wind turbine with coaxial contra-rotating concept. *Renew Energy* 2018; *115*: 353–361.
- [21] Eltayesh A, Castellani F, Burlando M, Hanna MB, Huzayyin AS, El-Batsh HM, Becchetti M. Experimental and numerical investigation of the effect of blade number on the aerodynamic performance of a small-scale horizontal axis wind turbine. *Alexandria Eng J* 2021; 60(4): 3931–3944.
- [22] Murthy KSR, Rahi OP. A comprehensive review of wind resource assessment. *Renew Sustain Energy Rev* 2017; 72: 1320–1342.
- [23] Zanforlin S, Letizia S. Improving the performance of wind turbines in urban environment by integrating the action of a diffuser with the aerodynamics of the rooftops. *Energy Procedia* 2015; 82: 774–781.
- [24] Arumugam P, Ramalingam V, Bhaganagar K. A pathway towards sustainable development of small capacity horizontal axis wind turbines–Identification of influencing design parameters & their role on performance analysis. *Sustain Energy Technol Assess* 2021; 44: 101019.
- [25] Sunny KA, Kumar P, Kumar NM. Experimental study on novel curved blade vertical axis wind turbines. *Results Eng* 2020; 7: 100149.

- [26] El-Shahat A, Hasan M, Abdelaziz AY. Micro-small-scale horizontal axis wind turbine design and performance analysis for micro-grids applications. In: *Smart Microgrids: From Design to Laboratory-Scale Implementation*, 2019. pp. 65–117.
- [27] Jouchi AA, Pourrajabian A, Rahgozar S, Dehghan M. A novel and economic rotor hub configuration for small wind turbines. *Sustain Energy Technol Assess* 2021; 47: 101344.
- [28] Kassa BY, Baheta AT, Beyene A. Current trends and innovations in enhancing the aerodynamic performance of small-scale, horizontal axis wind turbines: A review. *ASME Open J Eng* 2024; 3.
- [29] Chong WT, Gwani M, Tan CJ, Muzammil WK, Poh SC, Wong KH. Design and testing of a novel building integrated cross axis wind turbine. *Appl Sci* 2017; 7(3): 251.
- [30] Recharge news. Norwegian start-up's giant 117-turbine floating wind design adds \$1M to warchest for launch [Internet]. Available from: https://www.rechargenews.com/wind/norwegian-start-ups-giant-117-turbine-floating-wind-design-adds-1m-to-warchest-for-launch/2-1-1402436. Accessed 24 July 2024.
- [31] Chen YJ, Shiah YC. Experiments on the performance of small horizontal axis wind turbine with passive pitch control by disk pulley. *Energies* 2016; *9*(5): 353.
- [32] Corbalán PA, Chiang LE. Fast Power Coefficient vs. Tip–Speed Ratio Curves for Small Wind Turbines with Single-Variable Measurements Following a Single Test Run. *Energies* 2024; *17*(5): 1199.
- [33] Gribkov SV. Technique for testing small wind turbines by method of acceleration in the wind tunnel and in the field. In: *IOP Conference Series: Earth and Environmental Science* 2021 Mar; 689(1): 012019. IOP Publishing.
- [34] Ighodaro O, Akhihiero D. Modeling and performance analysis of a small horizontal axis wind turbine. *J Energy Res Technol* 2021; 143(3): 031301.
- [35] Zakaria MY, Pereira DA, Hajj MR. Experimental investigation and performance modeling of centimeter-scale micro-wind turbine energy harvesters. *J Wind Eng Ind Aerodyn* 2015; *147*: 58–65.
- [36] Jackson RS, Amano R. Experimental study and simulation of a small-scale horizontal-axis wind turbine. *J Energy Res Technol* 2017; *139*(5): 051207.
- [37] Kumar PM, Sivalingam K, Narasimalu S, Lim TC, Ramakrishna S, Wei H. A review on the evolution of Darrieus vertical axis wind turbine: Small wind turbines. *J Power Energy Eng* 2019; 7(4): 27–44.
- [38] Bhowon A, Abo-Al-Ez KM, Adonis M. Variable-speed wind turbines for grid frequency support: A systematic literature review. *Mathematics* 2022; *10*(19): 3586.
- [39] Zoucha J, Crespo C, Wolf H, Aboy M. Review of recent patents on vertical-axis wind turbines (VAWTs). *Recent Patents Eng* 2023; 17(4): 3–15.
- [40] Fonseca LM, Rodrigues GV, Savi MA. An overview of the mechanical description of origami-inspired systems and structures. *Int J Mech Sci* 2022; 223: 107316.
- [41] Liu H, James RD. Design of origami structures with curved tiles between the creases. *J Mech Phys Solids* 2024; 185: 105559.
- [42] Cozmei M, Hasseler T, Kinyon E, Wallace R, Deleo AA, Salviato M. Aerogami: Composite origami structures as active aerodynamic control. *Compos Part B Eng* 2020; *184*: 107719.
- [43] Aeromine. The motionless wind energy system [Internet]. Available from: https://aerominetechnologies.com/. Accessed 24 July 2024.
- [44] Ventum Dynamics. VX175 rooftop friendly wind turbine [Internet]. Available from: https://ventumdynamics.com/. Accessed 24 July 2024.
- [45] Guo Y, Ru P, Su J, Anadon LD. Not in my backyard, but not far away from me: Local acceptance of wind power in China. *Energy* 2015; 82: 722–733.
- [46] Petrova MA. NIMBYism revisited: Public acceptance of wind energy in the United States. *WIREs Clim Change* 2013; *4*(6): 575–601.
- [47] FlashForge Creator 3. [Internet]. Available from: https://flashforge-usa.com/products/shop-flashforge-creator-3-pro-independent-dual-extruder-3d-printer. Accessed 24 July 2024.
- [48] GUNT. HM 170 open wind tunnel [Internet]. Available from: https://www.gunt.de/en/products/open-wind-tunnel/070.17000/hm170/glct-1:pa-148:pr-769. Accessed 24 July 2024.
- [49] Çengel YA. Fluid Mechanics: Fundamentals and Applications. ISE Paperback ed. New York: McGraw-Hill Education, 2024.
- [50] Ohya Y, Karasudani T, Sakurai A, Abe KI, Inoue M. Development of a shrouded wind turbine with a flanged diffuser. *J Wind Eng Ind Aerodyn* 2008; *96*(5): 524–539.